Time-reversal symmetry-breaking nematic superconductivity in FeSe

Jian Kang,[1,*] Andrey V. Chubukov,[2] and Rafael M. Fernandes[2]
[1]*National High Magnetic Field Laboratory, Florida State University, Tallahassee, Florida 32304, USA*
[2]*School of Physics and Astronomy, University of Minnesota, Minneapolis, Minnesota 55455, USA*

(Received 17 May 2018; published 20 August 2018)

FeSe is a unique member of the family of iron-based superconductors, not only because of the high values of T_c in FeSe monolayer, but also because in bulk FeSe superconductivity emerges inside a nematic phase without competing with long-range magnetic order. Near T_c, superconducting order necessarily has $s+d$ symmetry, because nematic order couples linearly the s-wave and d-wave harmonics of the superconducting order parameter. Here we argue that the near-degeneracy between s-wave and d-wave pairing instabilities in FeSe, combined with the sign-change of the nematic order parameter between hole and electron pockets, allows the superconducting order to break time-reversal symmetry at a temperature $T^* < T_c$. The transition from an $s+d$ state to an $s+e^{i\alpha}d$ state should give rise to a peak in the specific heat and to the emergence of a soft collective mode that can be potentially detected by Raman spectroscopy.

DOI: 10.1103/PhysRevB.98.064508

I. INTRODUCTION

The discovery of FeSe brought renewed interest in the field of unconventional superconductors, not only because FeSe-based compounds display the highest superconducting (SC) transition temperatures among all iron-superconductors, but also because of their unique phase diagram [1]. Indeed, in contrast to most Fe-based compounds, bulk FeSe undergoes nematic and SC transitions without displaying long-range antiferromagnetic order [2,3]. The microscopic origin of this unusual behavior has been the subject of intense debates [4–10]. Regardless of the microscopic origin of nematicity, the phase diagrams of pure and doped FeSe provide a remarkable opportunity to investigate the interplay between nematicity and superconductivity without the interfering effects of the antiferromagnetic order observed near the onset of nematicity in other iron-based materials [11,12].

It is well established that nematic and SC orders coexist microscopically in FeSe, with the former onsetting at $T_s \approx 90$ K [13,14] and the latter at $T_c \approx 8$ K [13]. Recent experimental [15–25] and theoretical works [26–29] have highlighted how the modifications in the orbital compositions of the Fermi surfaces below the nematic transition influence the SC gap structure, and particularly the gap anisotropy on both hole and electron pockets. These gap anisotropies have been observed directly by Angle resolved photoemission spectroscopy (ARPES) [15–19] and scanning tunneling microscopy (STM) [20–22], and also indirectly in specific heat and thermal conductivity measurements [23–25].

General models for the pairing interaction in Fe-based SC have revealed closely competing s^{+-} and d-wave pairing channels, with the latter even winning over the former in certain models [30–38]. However, in Fe-pnictides, such near-degeneracy holds only far enough from the magnetically ordered phase, otherwise the $(\pi,0)/(0,\pi)$ stripe-type magnetic fluctuations favor s^{+-} pairing [39]. In FeSe, the situation is different. First, there is no magnetic order. If one takes this as evidence that magnetic fluctuations are not strong and treats the pairing within the Kohn-Luttinger scenario, one finds (see below) that s-wave and d-wave pairing amplitudes are quite comparable. Second, if one takes a different point of view and assumes that magnetic fluctuations in FeSe are strong enough to justify a spin-fluctuation approach, one still has to include into consideration not only $(\pi,0)/(0,\pi)$ fluctuations, but also (π,π) Néel-type magnetic fluctuations [40,41], as both have been observed in neutron scattering [42]. The stripe magnetic fluctuations enhance the pairing strength in the s^{+-} pairing channel, and the (π,π) fluctuations do the same in the d-wave channel [38]. The existence of both fluctuations again keeps the s^{+-} and d-wave pairing amplitudes comparable.

It is well known that proximate s^{+-} and d-wave states can lead to the emergence at low enough T of an exotic SC state that breaks time-reversal symmetry (TRS): the $s+id$ state. It emerges as the lowest-energy state because it gaps out all states on the Fermi surfaces and by this maximizes the gain of the condensation energy. An $s+id$ state has been proposed to exist in strongly hole-doped and strongly electron-doped Fe-pnictides [31–33,35,38], but it has not been yet unambiguously detected in experiments. As we just said, in FeSe, s^{+-} and d-wave states are likely closer than in Fe-pnictides [26], so FeSe seems a natural candidate to search for $s+id$ order. However, there is a caveat—the nematic order couples linearly the s-wave and d-wave channels. Because of this coupling, the SC order parameter near T_c necessarily has $s+d$ symmetry rather than $s+id$ [34,36,37]. An $s+d$ SC order preserves TRS and just changes the anisotropy of the gap function. If the linear coupling between s-wave and d-wave order parameters is strong enough, $s+d$ state persists down to $T=0$. If, however, it is weak, the system may undergo a transition at some $T < T_c$ into a time-reversal symmetry breaking (TRSB) state (see Fig. 1).

*jian.kang@fsu.edu

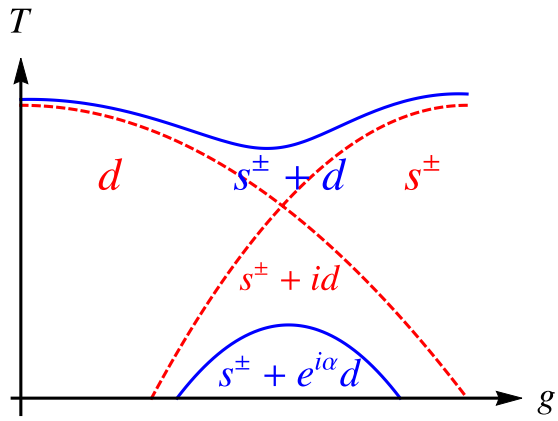

FIG. 1. Schematic figure summarizing our main results. As function of a tuning parameter g (which in our paper is the ratio between intraorbital and interorbital interband pairing interactions), the superconducting state changes from d-wave to s^{+-}-wave in the tetragonal phase, giving rise to an $s+id$ state near the degeneracy point (dashed red curves). In the nematic phase, the superconducting state becomes $s+d$ near T_c, which is enhanced near the s-wave/d-wave degeneracy point. At low temperatures, an $s+e^{i\alpha}d$ state can be stabilized (solid blue curves). Such an exotic state, which breaks both time-reversal and tetragonal symmetries, is much more favored for a sign-changing nematic state, as compared to a sign-preserving nematic state.

In general, the gap function of a SC state with s-wave and d-wave components is parametrized by

$$\Delta = \Delta_s + e^{i\alpha}\Delta_d. \tag{1}$$

For definiteness, we assume that both Δ_s and Δ_d are real. The relevant parameter in Eq. (1) is the relative phase $0 \leqslant \alpha \leqslant \pi$ between the two order parameters. In the $s+d$ state, $\alpha = 0$ or π, whereas in $s+id$ state $\alpha = \pm\pi/2$. Other values of α describe nematic SC states which also break TRS.

In this paper, we analyze the gap structure of FeSe below T_c by solving the set of non-linear gap equations on the different hole and electron pockets. We take as input the fact that in FeSe the nematic order parameter changes sign between hole and electron pockets [4,19,43,44]. We argue that for a sign-changing nematic order, the linear coupling between s-wave and d-wave gap components is much smaller than it would be if nematic order was sign-preserving. We analyze the gap structure and show that for parameters appropriate for FeSe it is quite likely that below some $T^* < T_c$, α becomes different than 0 or π, i.e., the system undergoes a transition into TRSB state.

Such a SC-to-SC transition is manifested by the softening of the collective mode associated with the fluctuations of α. This can be probed by Raman spectroscopy. The signatures of the transition into the TRSB state can also be found by measuring thermodynamic quantities, such as the specific heat. Interestingly, recent specific heat measurements on FeSe have reported a peak well below T_c [45]. We conjecture that this feature could be due to the formation of the TRSB state.

The paper is organized as follows. In Sec. II, we introduce our microscopic model with hole and electron pockets and on-site Hund and Hubbard interactions. We obtain the effective pairing interactions in the s^{+-} and d-wave channels within the Kohn-Luttinger formalism and rationalize an effective model with s-wave and d-wave attractive interactions of comparable magnitudes. In Sec. III, we study the pairing in the tetragonal phase and obtain the TRSB $s+id$ state for some range of system parameters. In Sec. IV, we analyze the pairing in the presence of nematic order. We show that near T_c the pairing symmetry is necessarily $s+d$, but TRSB state may still emerge at a lower T. In this section, we also compare the effects of sign-changing and sign-preserving nematic order. We argue that TRSB state is substantially more likely when the nematic order is sign-changing, as in FeSe. In Sec. V, we discuss experimental signatures of the transition into the TRSB state, in particular the softening of the collective mode associated with the fluctuations of the relative phase between s-wave and d-wave order parameters. Section VI presents our conclusions. Appendices A and B contain additional details not discussed in the main text.

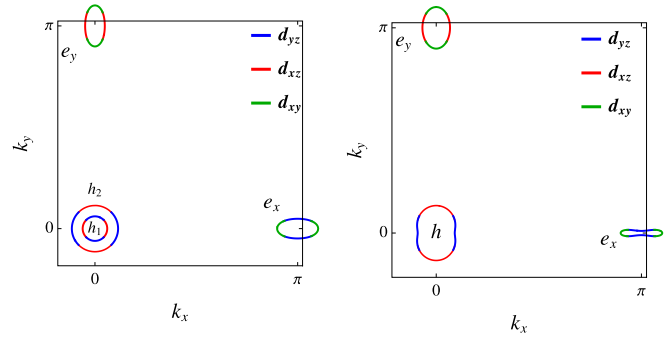

FIG. 2. The Fermi surface and its orbital content in the tetragonal (left) and nematic (right) phases of FeSe in the 1-Fe Brillouin zone. In the tetragonal phase, there are two hole pockets centered at $\Gamma/Z = (0,0)$ and two electron pockets X and Y centered at $(\pi,0)$ and $(0,\pi)$. Deep in the nematic phase there is one hole (h) pocket centered at $\Gamma/Z = (0,0)$ (another sinks below the Fermi level) and two electron pockets X and Y centered at $(\pi,0)$ and $(0,\pi)$, respectively. STM and ARPES data [15,20] show that the h pocket is an ellipse elongated along Y, and that the X electron pocket has a peanut-type form with the minor axis along the Y direction.

II. MICROSCOPIC MODEL

A. Noninteracting terms

Our microscopic Hamiltonian contains a noninteracting part, $\mathcal{H}_0$, and an interacting part, $\mathcal{H}_{\rm int}$. The former is constructed based on ARPES measurements, which find, above the nematic transition temperature T_s, two small hole pockets at the center of the Brillouin zone and two small electron pockets centered at $\mathbf{Q}_X = (\pi,0)$ and $\mathbf{Q}_Y = (0,\pi)$ in the Fe-only Brillouin zone [17,46–48]. We show the Fermi pockets and orbital content of excitations around the pockets in Fig. 2.

The spectral weight of excitations near the hole pockets comes predominantly from the d_{xz} and d_{yz} Fe orbitals. As a result, the hole-band operators $h_{1,\mathbf{k}}$ and $h_{2,\mathbf{k}}$ can be expressed in terms of the orbital operators $d_{xz,\mathbf{k}}$ and $d_{yz,\mathbf{k}}$ as [49,50]

$$\begin{aligned} h_{1,\mathbf{k}} &= i(d_{xz,\mathbf{k}}\cos\theta_{\mathbf{k}} + d_{yz,\mathbf{k}}\sin\theta_{\mathbf{k}}),\\ h_{2,\mathbf{k}} &= i(-d_{xz,\mathbf{k}}\sin\theta_{\mathbf{k}} + d_{yz,\mathbf{k}}\cos\theta_{\mathbf{k}}). \end{aligned} \tag{2}$$

The imaginary prefactors are introduced for convenience, as later we will search for TRSB solutions of the gap equations. The relationship between the Bogoliubov parameter $\theta_{\mathbf{k}}$ and the polar angle θ around the hole pockets (measured with respect to k_x) depends on the tight-binding parameters. For our purposes, it is sufficient to consider the special case of circular hole pockets, in which case $\theta_{\mathbf{k}} = \theta$. Because the hole pockets are small, we can approximate their dispersions as parabolic, $\varepsilon_{h_i} = \mu_h - k^2/2m_i$, with $m_2 > m_1$.

The electron pockets are predominantly formed out of $d_{xz/yz}$ and d_{xy} orbitals. We describe them by the operators $e_{X/Y,\mathbf{k}}$. We use as input the results of earlier renormalization group (RG) studies [51] that the interactions involving fermions from d_{xy} orbitals flow to smaller values than the ones involving fermions from d_{xz} and d_{yz} orbitals. The smallness of the interactions involving d_{xy} orbitals has also been proposed in strong-coupling approaches [52–54] and phenomenologically in recent studies of the linearized gap equation in FeSe [20,28]. To simplify the analysis, we then neglect fermions from the d_{xy} orbital in the pairing problem and approximate the excitations near the X pocket as d_{yz} ($e_{X,\mathbf{k}} = d_{yz,\mathbf{k}+\mathbf{Q}_X}$) and near the Y pocket as d_{xz} ($e_{Y,\mathbf{k}} = d_{xz,\mathbf{k}+\mathbf{Q}_Y}$), with electron-band dispersions $\varepsilon_{X,Y} = -\mu_e + k_x^2/(2m_{X,Y}) + k_y^2/(2m_{Y,X})$. This approximation substantially simplifies the analysis of the transition into the TRSB state at T^*. The inclusion of d_{xy} orbitals does not change the main results, as it only shifts the value of T^*. By the same reason, we also neglect spin-orbit coupling [55] and the variation of the size of the hole pockets along the k_z direction. The k_z variation is relevant for the understanding of the orbital composition of the hole pockets in the nematic phase and of the gap anisotropy in the $s+d$ phase [17,19,28], but does not qualitatively alter the physics of the transition into the TRSB state.

B. Interaction terms

The interacting part of the Hamiltonian $\mathcal{H}_{\rm int}$ is responsible for the SC instability. Let us first analyze SC in the absence of nematic order. As discussed in the introduction, there are two approaches to the pairing instability. One is to start with bare interactions, such as the on-site Hund and Hubbard interactions, and analyze the pairing to second order in perturbation theory (the Kohn-Luttinger approach). Another is to adopt the semiphenomenological spin-fluctuation scenario and analyze the pairing mediated by spin fluctuations.

Within the first scenario, both s-wave and d-wave components of the interaction emerge when one converts from orbital to band basis using Eqs. (2). In the tetragonal phase, the effective BCS Hamiltonian factorizes between s- and d-channels. Symmetry analysis shows [4,50] there are three relevant pairing interactions: one between fermions on the two hole pockets, another between fermions on the two electron pockets, and the third between fermions on hole and on electron pockets. To be consistent with the notation in earlier works, we label these three interactions, respectively, as $U_4^{s(d)}$, $U_5^{s(d)}$, and $U_3^{s(d)}$.

To write the BCS Hamiltonian in a compact form, we follow Ref. [4] and introduce the pair operators

$$\kappa^e_{\mu\mu'} = e_{\mu\uparrow}e_{\mu'\downarrow}, \quad \kappa^h_{\mu\mu'} = h_{\mu\uparrow}h_{\mu'\downarrow}, \tag{3}$$

where $\mu = 1, 2$, $e_1 = e_Y$ and $e_2 = e_X$, and

$$\kappa_s^{e(h)} = \kappa_{11}^{e(h)} + \kappa_{22}^{e(h)},$$
$$\kappa_d^{e(h)} = \kappa_{11}^{e(h)} - \kappa_{22}^{e(h)}. \tag{4}$$

The pairing Hamiltonian is then given by

$$H_\kappa = H_{\kappa_s} + H_{\kappa_d}, \tag{5}$$

where

$$H_{\kappa_s} = U_5^s\left(\kappa_s^e\right)^\dagger\kappa_s^e + U_4^s\left(\kappa_s^h\right)^\dagger\kappa_s^h + U_3^s\left(\left(\kappa_s^e\right)^\dagger\kappa_s^h + \text{H.c.}\right), \tag{6}$$

$$H_{\kappa_d} = U_5^d\left(\kappa_d^e\right)^\dagger\kappa_d^e + U_4^d\left(\kappa_d^h\right)^\dagger\kappa_d^h + U_3^d\left(\left(\kappa_d^e\right)^\dagger\kappa_d^h + \text{H.c.}\right). \tag{7}$$

We assume momentarily that the densities of states on all pockets are equal to N_F. Introducing $u_i^{s(d)} = U_i^{s(d)}N_F/2$ and solving the BCS gap equations in s-wave and d-wave channels, we obtain two dimensionless couplings in each channel, corresponding to same-sign (denoted by s^{++} and d^{++}) or opposite-sign (denoted by s^{+-} and d^{+-}) gaps on electron and hole pockets. One of the two is repulsive for positive $U_i^{s(d)}$, whereas the other can be of either sign, depending on the interplay between the U_5, U_4, and U_3 interactions. These couplings are

$$\lambda^s = \frac{\left(u_3^s\right)^2 - u_4^s u_5^s}{u_4^s + u_5^s}, \tag{8}$$

$$\lambda^d = \frac{\left(u_3^d\right)^2 - u_4^d u_5^d}{u_4^d + 2u_5^d}. \tag{9}$$

Note that a positive λ implies attraction. Symmetry analysis shows [56] that λ^s corresponds to the s^{+-} channel and λ_d to the d^{++} channel.

The bare values of the interactions $U_i^{s(d)}$ are $U_5^s = U_4^s = U_3^s = (U+J)/2$, $U_5^d = U_4^d = U_3^d = (U-J)/2$. Substituting into Eqs. (8) and (9), we see that the couplings in both s and d channels vanish. A nonzero $\lambda^{s(d)}$ emerge when we include the renormalizations of the interactions between given fermions due to the presence of other fermions. If the system does not show a strong tendency toward a density-wave order, these renormalizations can be computed to second order in $u_i^{s(d)}$. Still, in systems with hole and electron pockets, some renormalizations are logarithmically singular, i.e., they depend on $L = \log W/E$, where W is the bandwidth and E is the energy at which we probe λ^s and λ^d. Keeping only the logarithmical terms, and extracting the renormalizations to order $(u_i^{s(d)})^2$ from the RG equations for the flow of the couplings [4], we obtain, in terms of U and J,

$$\lambda^s = 4U^2N_F^2(1 + J/U - 2J^2/U^2)L, \tag{10}$$

$$\lambda^d = \tfrac{8}{3}U^2N_F^2(1 - J/U + 2J^2/U^2)L. \tag{11}$$

We see that for $U > J$, both λ_s and λ_d are positive, i.e., the dressed couplings are attractive in both s-wave and d-wave channels. For large U/J, $\lambda^s > \lambda^d$, i.e., the s-wave channel is more attractive. However, for $0.65 < J/U < 1$, $\lambda^d > \lambda^s$, implying that the d-wave channel is more attractive. For nonequal densities of states on different pockets, the formulas are more complex, but the key result is the same: the couplings

λ^s and λ^d in s^{+-} and d^{++} channels vanish if we use bare interactions but become positive (attractive) when we include the renormalizations of the interactions to order $(u_i^{s(d)})^2$.

From a physics perspective, $\lambda^{s(d)}$ becomes attractive because the corrections to order $(u_i^{s(d)})^2$ increase the interpocket interaction u_3 compared to the interactions between fermions near only hole or only electron pockets. This generally moves the system toward a stripe magnetic order. For large enough U/J, this predominantly increases the interaction in the s^{+-} channel, but when U and J are comparable, this may increase even more the pairing interaction in the d-wave channel. Note that this is entirely due to the enhancement of the interaction at the stripe wave vectors $(0,\pi)/(\pi,0)$. The (π,π) interaction between the electron pockets is present as the interpocket component of the interaction $U_5^{s(d)}$, but to logarithmical accuracy it is not enhanced compared to the intrapocket component of $U_5^{s(d)}$.

An alternative to the Kohn-Luttinger approach is the phenomenological spin-fluctuation approach. Here, one takes as input the fact that stripe and Neel magnetic fluctuations are enhanced and considers only interpocket interactions with momentum transfer $(\pi,0)/(0,\pi)$ and (π,π). In the absence of competing intrapocket interactions, λ^c and λ^d are definitely positive. When U/J is large, $(\pi,0)/(0,\pi)$ fluctuations favor s^{+-} pairing. However, (π,π) fluctuations favor a state with sign-changing gaps between the electron pockets, which by symmetry is d-wave. The interplay between λ^s and λ^d is then determined by the details of spin-fluctuations near $(\pi,0)/(0,\pi)$ and (π,π) [34,38].

We see that in both Kohn-Luttinger and spin-fluctuation approaches, the couplings λ^s and λ^d are attractive, and their ratio depends on microscopic details. Hereafter, we adopt a combined approach in which we take the elements of both Kohn-Luttinger and spin-fluctuation treatments. Specifically, we keep in the interaction Hamiltonian one intraorbital, interband interaction, V, and two interorbital, interband interactions, W_1 and W_2. The interaction Hamiltonian, projected onto the pairing channel, is

$$\begin{aligned}\mathcal{H}_{\rm SC} = & V\sum_{\mathbf{k},\mu} d^\dagger_{\mu,\mathbf{k}\uparrow} d^\dagger_{\mu,-\mathbf{k}\downarrow} d_{\mu,\mathbf{k}'+\mathbf{Q}_\mu\downarrow} d_{\mu,-\mathbf{k}'+\mathbf{Q}_\mu\uparrow} \\ & + W_1 \sum_{\mathbf{k},\mu\neq\nu} d^\dagger_{\mu,\mathbf{k}\uparrow} d^\dagger_{\mu,-\mathbf{k}\downarrow} d_{\nu,\mathbf{k}'+\mathbf{Q}_\nu\downarrow} d_{\nu,-\mathbf{k}'+\mathbf{Q}_\nu\uparrow} \\ & + W_2 \sum_{\mathbf{k},\mu\neq\nu} d^\dagger_{\mu,\mathbf{k}+\mathbf{Q}_\mu\uparrow} d^\dagger_{\mu,-\mathbf{k}+\mathbf{Q}_\mu\downarrow} d_{\nu,\mathbf{k}'+\mathbf{Q}_\nu\downarrow} d_{\nu,-\mathbf{k}'+\mathbf{Q}_\nu\uparrow},\end{aligned} \tag{12}$$

where $\mu,\nu = xz,\ yz$, $Q_\mu = (\pi,0)$ for $\mu = yz$ and $Q_\mu = (0,\pi)$ for $\mu = xz$. The terms V and W_1 are interactions between hole and electron pockets, while W_2 term describes interaction between the two electron pockets. Interaction V acts within a given orbital (the same index μ for all fermions), hence it is intraorbital, while momentum changes between $\boldsymbol{k}$ and $\boldsymbol{k}+\boldsymbol{Q}$, hence it is interband. The interactions $W_{1,2}$ act between fermions from different orbitals, hence, they are interorbital, and the momentum changes between $\boldsymbol{k}$ and $\boldsymbol{k}+\boldsymbol{Q}$ for W_1 and between $\boldsymbol{k}$ and $\boldsymbol{k}+(\pi,\pi)$ for W_2, hence these are also interband interactions.

Equation (12) together with the kinetic energy term describe the pairing in the tetragonal phase. In the nematic phase below T_s, two new effects emerge. First, the kinetic energy changes because nematicity (regardless of its origin) breaks C_4 lattice rotational symmetry and gives rise to orbital order, which distinguishes between d_{xz} and d_{yz} orbitals. The corresponding order parameter is $\Phi(\mathbf{k}) = \langle n_{xz,\mathbf{k}}\rangle - \langle n_{yz,\mathbf{k}}\rangle$, where n_i is the occupation number operator. This order parameter has two components: one on hole pockets, $\Phi_h \equiv \Phi(\mathbf{k}=0)$, another on electron pockets, $\Phi_e \equiv \Phi(\mathbf{Q}_X) = -\Phi(\mathbf{Q}_Y)$. The orbital order with Φ_h and Φ_e adds an additional term to the kinetic energy in the form

$$\begin{aligned}\mathcal{H}_{\rm nem} = & \sum_{\mathbf{k}\sigma} \Phi_h (d^\dagger_{xz,\mathbf{k}\sigma} d_{xz,\mathbf{k}\sigma} - d^\dagger_{yz,\mathbf{k}\sigma} d_{yz,\mathbf{k}\sigma}) \\ & + \sum_{\mathbf{k}\sigma} \Phi_e (d^\dagger_{xz,\mathbf{k}+\mathbf{Q}_Y\sigma} d_{xz,\mathbf{k}+\mathbf{Q}_Y\sigma} - d^\dagger_{yz,\mathbf{k}+\mathbf{Q}_X\sigma} d_{yz,\mathbf{k}+\mathbf{Q}_X\sigma}).\end{aligned} \tag{13}$$

Orbital order modifies the shapes of the hole and electron pockets: the hole pockets become elliptical and one of the electron pockets becomes peanutlike-shaped. This has been observed in ARPES and STM experiments [15–22]. The observed geometry of the pockets is reproduced if Φ_h and Φ_e have opposite signs [19,44]. In common terminology, such an order is called sign-changing nematic order. Orbital order also modifies the s-wave and d-wave components of the pairing interaction once one converts it from orbital to band basis, because in the presence of Eq. (13), the Bogoliubov parameters θ_k in Eqs. (2) no longer coincides with the polar angle around the hole pocket [36].

The second effect of nematicity is the splitting of the pairing interaction between xz and yz orbitals already in the orbital basis, i.e., in Eq. (12). In some earlier works this effect has been included either phenomenologically [20,27], or semiphenomenologically, by invoking spin-nematic scenario and assuming stronger spin fluctuations at $(\pi,0)$ in the nematic phase [19,29,34,57]. In our study, we neglect this effect on the grounds that (i) in the band basis (which we will use to study pairing) its result is qualitatively similar to nematicity-induced change of the Bogoliubov parameter θ_k and (ii) the strength of the d_{xz}/d_{yz} splitting of the pairing interaction in the orbital basis has been argued [52] to be quite small if the nematic order emerges as a spontaneous orbital order (a d-wave Pomeranchuk instability). It can be potentially larger, though, if the nematic order in FeSe has magnetic origin, like in Fe-pnictides.

III. SUPERCONDUCTING INSTABILITIES IN THE TETRAGONAL PHASE

To set the stage, we first solve the pairing problem in the tetragonal phase, where $\Phi_h = \Phi_e = 0$. To model the situation of FeSe, our first goal is to find the region in the three-dimensional parameter space of interactions (V, W_1, W_2), where the two leading SC instabilities, s^{+-} and d-wave, are comparable. To simplify the calculations, we hereafter set $W_1 = W_2$. We argue that this will not affect our main conclusions because we consider only two pairing channels and only need two effective pairing interactions (two couplings), which

are combinations of V, W_1, and W_2. For $W_1 = W_2 = W$, we can express these two couplings in terms of two system parameters and analyze the interplay between s-wave and d-wave pairings. Keeping $W_1 \neq W_2$ will not give rise to qualitative change phases because the interplay between s-wave and d-wave is still determined by the ratio of the two effective couplings made out of V, W_1 and W_2.

Denoting the gap functions at each band a by $\Delta_a(\theta)$, we obtain the BCS-like nonlinear gap equations in the form

$$-\Delta_{h_1}(\theta_1) = T\sum_n \left\{ \int \frac{d^2k_X}{(2\pi)^2} \frac{V\sin^2\theta_1 + W\cos^2\theta_1}{\epsilon_X^2 + \omega_n^2 + |\Delta_{e_X}|^2}\Delta_{e_X} + \int \frac{d^2k_Y}{(2\pi)^2} \frac{W\sin^2\theta_1 + V\cos^2\theta_1}{\epsilon_Y^2 + \omega_n^2 + |\Delta_{e_Y}|^2}\Delta_{e_Y} \right\}, \tag{14}$$

$$-\Delta_{h_2}(\theta_2) = T\sum_n \left\{ \int \frac{d^2k_X}{(2\pi)^2} \frac{V\cos^2\theta_2 + W\sin^2\theta_2}{\epsilon_X^2 + \omega_n^2 + |\Delta_X|^2}\Delta_{e_X} + \int \frac{d^2k_Y}{(2\pi)^2} \frac{W\cos^2\theta_2 + V\sin^2\theta_2}{\epsilon_Y^2 + \omega_n^2 + |\Delta_{e_Y}|^2}\Delta_{e_Y} \right\}, \tag{15}$$

$$\begin{aligned} -\Delta_{e_X}(\boldsymbol{k}_X) = T\sum_n \Bigg\{ & \int \frac{d^2k_1}{(2\pi)^2} \frac{V\sin^2\theta_1 + W\cos^2\theta_1}{\epsilon_1^2 + \omega_n^2 + |\Delta_{h_1}|^2}\Delta_{h_1}(\theta_1) + \int \frac{d^2k_2}{(2\pi)^2} \frac{V\cos^2\theta_2 + W\sin^2\theta_2}{\epsilon_2^2 + \omega_n^2 + |\Delta_{h_2}|^2}\Delta_{h_2}(\theta_2) \\ & + W\int \frac{d^2k_Y}{(2\pi)^2} \frac{\Delta_{e_Y}}{\epsilon_Y^2 + \omega_n^2 + |\Delta_{e_Y}|^2} \Bigg\}, \end{aligned} \tag{16}$$

$$\begin{aligned} -\Delta_{e_Y}(\boldsymbol{k}_Y) = T\sum_n \Bigg\{ & \int \frac{d^2k_1}{(2\pi)^2} \frac{V\cos^2\theta_1 + W\sin^2\theta_1}{\epsilon_1^2 + \omega_n^2 + |\Delta_{h_1}|^2}\Delta_{h_1}(\theta_1) + \int \frac{d^2k_2}{(2\pi)^2} \frac{V\sin^2\theta_2 + W\cos^2\theta_2}{\epsilon_2^2 + \omega_n^2 + |\Delta_{h_2}|^2}\Delta_{h_2}(\theta_2) \\ & + W\int \frac{d^2k_X}{(2\pi)^2} \frac{\Delta_{e_X}}{\epsilon_X^2 + \omega_n^2 + |\Delta_{e_X}|^2} \Bigg\}. \end{aligned} \tag{17}$$

The gaps can be parametrized as

$$\begin{aligned} \Delta_{h_1} &= \Delta_1\sin^2\theta_1 + \Delta_2\cos^2\theta_1, \\ \Delta_{h_2} &= \Delta_1\cos^2\theta_2 + \Delta_2\sin^2\theta_2, \\ \Delta_{e_X} &= \Delta_X, \quad \Delta_{e_Y} = \Delta_Y. \end{aligned} \tag{18}$$

The solutions can be decomposed into the two orthogonal channels: the s^{+-}-wave state, corresponding to $\Delta_X = \Delta_Y = \Delta_e^s$ and $\Delta_1 = \Delta_2 = \Delta_h^s$ of opposite signs, and the d-wave state, corresponding to $\Delta_X = -\Delta_Y = \Delta_e^d$ and $\Delta_1 = -\Delta_2 = \Delta_h^d$, leading to $\Delta_{h_1} = -\Delta_{h_2} = \Delta_h^d\cos 2\theta_h$.

Near T_c, we can linearize the gap equations and use $T\sum_n \int d\boldsymbol{k} \frac{1}{\omega_n^2 + \epsilon_{a,\boldsymbol{k}}^2} \approx \frac{N_a}{2}\ln\frac{\sqrt{\Lambda\mu_a}}{T}$, where Λ is the high-energy cutoff associated with the pairing interaction and μ_a is the chemical potential of band a. Here, N_a is the density of states at the Fermi level. Fixing W to be $W = 0.5$ eV and solving for T_c for varying V, we find a transition from d-wave to s^{+-} upon increasing V, as shown in Fig. 3. The values of all the dispersion parameters are listed in Appendix A, and are consistent with those used in our previous work [28].

We also solve the gap equations at $T = 0$. To search for TRSB solutions, we introduce a relative phase between the gaps Δ_X and Δ_Y, which is related to the relative phase α between the s^{+-}-wave and d-wave gaps, Eq. (1). As shown in Fig. 3, we find that near the degeneracy point between the s^{+-} and d-wave states, $0.3 \lesssim V/W \lesssim 0.4$, the gap structure breaks TRS at $T = 0$, as signaled by the fact that $\alpha = \pm\pi/2$ in this regime. Note that α is not well defined in the other parameter ranges in which s^{+-} and d-wave SC do not coexist. The resulting schematic phase diagram at all temperatures is then that shown in Fig. 1. The presence of the spin orbital coupling and the inclusion of d_{xy} orbital on the electron pockets will only change the value of V/W when the two pairing instabilities are degenerate. The TRSB SC state still emerges when V/W is close to the degenerate value.

IV. SUPERCONDUCTING INSTABILITIES IN THE NEMATIC PHASE

We next solve the pairing problem in the fully reconstructed nematic Fermi surface. The onset of the nematic order, described by Eq. (13), has important effects on the low-energy electronic spectrum. For the states near the hole pockets, we follow earlier works [28,29] and introduce the Nambu operators $\Psi_{\mathbf{k}\sigma}^\dagger = (d_{xz,\mathbf{k}\sigma}^\dagger \quad d_{yz,\mathbf{k}\sigma}^\dagger)$ and write the quadratic Hamiltonian as $\hat{\mathcal{H}}_h = \sum_{\mathbf{k}\sigma} \Psi_{\mathbf{k}\sigma}^\dagger \hat{H}_h(\mathbf{k})\Psi_{\mathbf{k}\sigma}$, with

$$\hat{H}_h(\mathbf{k}) = \hat{\tau}_0\varepsilon_{h_+,\mathbf{k}} + \hat{\tau}_1\varepsilon_{h_-,\mathbf{k}}\sin 2\theta_{\mathbf{k}} + \hat{\tau}_3(\Phi_h + \varepsilon_{h_-,\mathbf{k}}\cos 2\theta).$$

Here, $\hat{\tau}_i$ are Pauli matrices in Nambu space, $\theta_{\mathbf{k}}$ is the parameter in the transformation from orbital to band representation (see below), and $\varepsilon_{h_\pm,\mathbf{k}} = (\varepsilon_{h_1,\mathbf{k}} \pm \varepsilon_{h_2,\mathbf{k}})/2$. A nonzero nematic order parameter Φ_h splits the top of the two hole bands and distort the hole pockets, whose new dispersions become $E_\pm = \varepsilon_{h_+} \pm \sqrt{\Phi_h^2 + \varepsilon_{h_-}^2 - 2\Phi_h\varepsilon_{h_-}\cos 2\theta}$ (here and below we skip subindex $\mathbf{k}$). To capture the experimental result that one of the pockets is sunk below the Fermi level [47], we set $\Phi_h > \mu_h$, and focus only on the E_+ dispersion for the outer pocket. In terms of the original orbital operators, the band operator for the outer pocket $h_2 \equiv h$ is still given by $h = i(-d_{xz}\sin\theta + d_{yz}\cos\theta)$, but the transformation coefficients

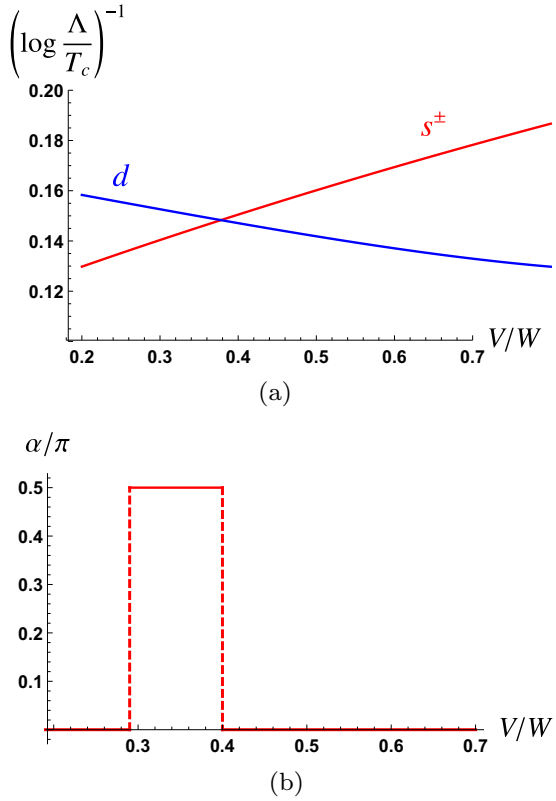

FIG. 3. (a) The two leading eigenvalues $\lambda = (\ln(\Lambda/T))^{-1}$ of the linearized BCS gap equation at $T = T_c$ as function of the ratio V/W. Here, V is the intraorbital, interpocket interaction, and W is the interorbital, intrapocket interaction. When $V \ll W$, the leading pairing instability is d-wave. When $V \gg W$, the leading instability is s^{+-} pairing. (b) The phase difference α between the s^{+-}-wave and d-wave gaps at $T = 0$. When $V \gg W$ or $V \ll W$, the pairing is either purely s-wave or purely d-wave, and α is not well-defined. But when $V \sim W$, the system spontaneously breaks time-reversal symmetry by forming an $s + id$ state with $\alpha = \pm\pi/2$.

$\cos\theta$ and $\sin\theta$ are given by (see Ref. [28] for detail)

$$\sin^2\theta = \frac{1}{2}\left(1 + \frac{\Phi_h + \epsilon_{h_-}\cos 2\theta}{\sqrt{\Phi_h^2 + \epsilon_{h_-}^2 + 2\Phi_h\epsilon_{h_-}\cos 2\theta}}\right),$$

$$\cos^2\theta_{\mathbf{k}} = \frac{1}{2}\left(1 - \frac{\Phi_h + \epsilon_{h_-}\cos 2\theta}{\sqrt{\Phi_h^2 + \epsilon_{h_-}^2 + 2\Phi_h\epsilon_{h_-}\cos 2\theta}}\right).$$

The effect of nematicity on the electron pockets is more straightforward, as Φ_e simply shifts the bottom of the electron pockets centered at X and Y in opposite ways, giving rise to the new dispersions $E_{X/Y} = \varepsilon_{X/Y} \pm \Phi_e$. The parameters of the dispersion are fitted with ARPES data, and listed in Appendix A.

The gap equations are essentially the same as in the previous calculation, but with $\theta \to \theta_{\Phi_h}$ and $\mu_{e,X/Y} \to \mu_e \mp \Phi_e$. The solid and dashed red curves in Fig. 4 show T_c of the two leading pairing instabilities in our model with sign-changing nematicity, i.e., $\text{sign}(\Phi_h) = -\text{sign}(\Phi_e)$. These two instabilities correspond to the "bonding" and "antibonding" mixing of the

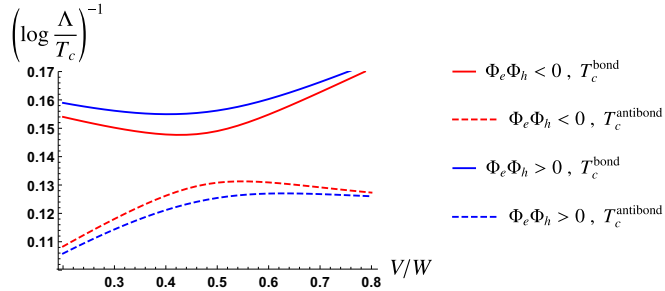

FIG. 4. Pairing instabilities in the nematic phase. The red solid and dashed curves refer to the sign-changing nematic state [$\text{sign}(\Phi_h) = -\text{sign}(\Phi_e)$], whereas the blue solid and dashed curves refer to the sign-preserving nematic state [$\text{sign}(\Phi_h) = \text{sign}(\Phi_e)$]. The splitting of the two leading pairing instabilities, corresponding to "bonding" and "antibonding" mixing of the s^{+-} and d-wave gaps, is smaller in the case of sign-changing nematicity, illustrating the reduced impact of nematic order on SC in this case.

s^{+-} and d-wave gaps, $\Delta_s \pm \Delta_d$. Observe that the degeneracy between the s^{+-} and d-wave gaps is lifted by the nematic order. It is also important to note that only the instability with a higher T_c is realized. Even though the second instability is not realized, the splitting between the two solutions brings important information on how strongly the nematic order lifts the degeneracy between the s^{+-} and d-wave states.

In this context, it is interesting to compare this case with the case of same-sign nematicity, shown by the blue curves in Fig. 4. The same parameters are used in this model except for the relative sign of the nematic order parameters Φ_h and Φ_e. We find that the splitting between the solutions corresponding to "bonding" and "antibonding" mixing between the s^{+-} and d-wave gaps is larger in the case of the same-sign nematic order parameters.

To gain a qualitative understanding of the difference between these two types of nematic order, we assume that the nematic order parameter is small, and apply a Ginzburg-Landau double-expansion in terms of the SC and nematic order parameters. Although the Ginzburg-Landau expansion is not technically valid in the case of FeSe, where $T_s \gg T_c$, it still provides qualitative insight for our numerical results. To leading order, the free energy is [34]

$$F(\Delta) = a_s|\Delta_s|^2 + a_d|\Delta_d|^2 - (\beta_h\Phi_h + \beta_e\Phi_e)(\Delta_s^*\Delta_d + \Delta_s\Delta_d^*) + O(|\Delta|^4), \tag{19}$$

where $a_s = T - T_c^{(s)}$ and $a_d = T - T_c^{(d)}$ refer to the SC transition temperatures in the tetragonal phase. The last term in the free energy is allowed because the product $\Delta_s^*\Delta_d$ changes sign under the rotation by $\pi/2$, i.e., has the same symmetry as a d-wave nematic order parameter, and the two order parameters of the same symmetry generally couple linearly in the free energy. This term mixes s-wave and the d-wave pairings. As a consequence, the single SC transition at the degeneracy point is split in two, corresponding to the "bonding" and "antibonding" $s \pm d$ states. The amplitude of the splitting ΔT_c between the bonding and antibonding mixing of the s-wave and d-wave

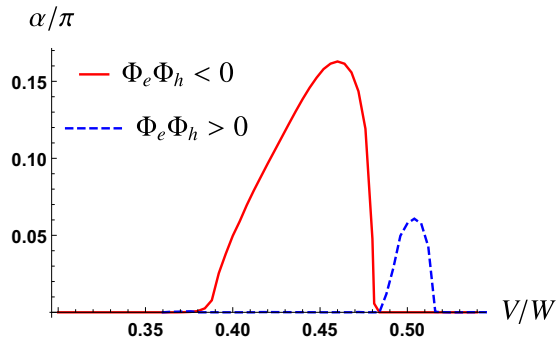

FIG. 5. The phase difference α between the s^{+-} and d-wave gaps at $T = 0$ in the nematic phase. When α is neither 0, π, or $\pi/2$ the SC state breaks both tetragonal and time-reversal symmetries. The solid red and dashed blue curves refer to the case of opposite-sign nematicity and same-sign nematicity, respectively. In the former, we find a much larger regime in which the SC state breaks time-reversal symmetry.

gaps is given by

$$\Delta T_c = \sqrt{\left(T_c^{(s)} - T_c^{(d)}\right)^2 + (\beta_h \Phi_h + \beta_e \Phi_e)^2}. \quad (20)$$

Therefore, if the coefficients β_h and β_e have the same sign, the splitting ΔT_c will be smaller for sign-changing nematicity ($\Phi_h \Phi_e < 0$) as compared to same-sign nematicity ($\Phi_h \Phi_e > 0$). The numerical results shown in Fig. 4 thus imply that the coefficients β_h and β_e have the same sign. Analytical calculations for the free energy, shown in Appendix B, confirm this result.

The fact that $|\beta_h \Phi_h + \beta_e \Phi_e|$ is smaller for sign-changing nematicity also suggests that a TRSB transition is more likely to take place at low temperatures in this case as compared to the case of same-sign nematicity. To see this, we consider higher-order terms in the free-energy expansion Eq. (19) that are sensitive to the relative phase α between the $s-$wave and $d-$wave gaps. The quartic order term is given by $\frac{\gamma}{4}(\Delta_s^* \Delta_d + \Delta_s \Delta_d^*)^2$, where $\gamma > 0$ favors $\alpha = \pi/2$ in the tetragonal phase, in agreement with our numerical results of the previous section. Minimization with respect to α in the nematic phase leads to the solutions $\alpha = 0, \pi$, corresponding to $s \pm d$, and

$$\alpha_0 = \arccos\left(\frac{\beta_h \Phi_h + \beta_e \Phi_e}{\gamma |\Delta_s||\Delta_d|}\right). \quad (21)$$

Close to T_c, the product $|\Delta_s||\Delta_d|$ is very small, and the $\alpha_0 \neq 0, \pi$ solution is not possible. However, as temperature decreases and the product $|\Delta_s||\Delta_d|$ increases, it is possible at $T^* < T_c$ for the free-energy minimum to move to $\alpha_0 \neq 0, \pi$, signaling a TRSB nematic SC state (denoted here by $s + e^{i\alpha} d$). Of course, smaller $|\beta_h \Phi_h + \beta_e \Phi_e|$ leads to a higher T^*. Thus, the regime where a TRSB nematic state is realized is expected to be larger in the case of sign-changing nematicity as compared to same-sign nematicity.

To go beyond this qualitative analysis, we also solved the gap equations at $T = 0$. The red curve in Fig. 5 shows the phase difference α between the s^{+-}-wave and d-wave gaps. We find $\alpha > 0$ for the range $0.39 \lesssim V/W \lesssim 0.48$, signaling that the system undergoes a SC-SC transition in which TRS is broken at a temperature T^* below T_c. While the regime with TRSB is narrower as compared to the tetragonal case, it is enhanced by the fact that Φ_e and Φ_h have opposite signs. Indeed, in Fig. 5, the blue curve shows α for the case in which Φ_e has the same sign as Φ_h. In this case, the parameter regime with TRSB SC is significantly reduced, in agreement with our qualitative analysis.

V. EXPERIMENTAL CONSEQUENCES: SPECIFIC HEAT AND SOFT MODE

The TRSB transition at T^* belongs to the Ising universality class, and as such it is manifested in several thermodynamic quantities, most notably as a peak in the specific heat. Because most of the entropy related to the SC degrees of freedom is released at T_c, the features in the specific heat at T^* are expected to be weaker than the jump at T_c. Interestingly, recent high-precision specific heat measurements in FeSe reported a peak in the specific heat at $T^* \approx 1$ K [45], which is consistent with a TRSB transition.

Direct evidence for TRSB could be obtained from measurements such as μSR and Kerr rotation, although the issues of TRSB Ising-like domains and induced current patterns may render these measurements challenging. We point out that recent STM data in FeSe has been interpreted in terms of a TRSB-SC state forming at the twin boundaries [58]. This observation is perfectly consistent with our results, as in the absence of nematic order, the relative phase α between the s-wave and d-wave gaps becomes $\pi/2$.

Alternatively, TRSB could be detected by probing the collective modes of FeSe. Since the TRSB transition takes place deep inside a nodeless SC state, the electronic spectrum is fully gapped. As a result, the SC collective modes are long-lived, as there are no quasiparticles to promote damping. To compute the collective modes, we need to evaluate the dynamic SC susceptibility. The latter can be obtained by expanding the gap around its mean-field value $\bar{\Delta}$, $\Delta = \bar{\Delta} + \delta$, and computing the one-loop bosonic self-energy diagram containing the coupling between the pairing fluctuations field δ and the fermions. In the single-band case, the bare pairing susceptibility is a 2×2 matrix whose diagonal components $\chi_n^i(\omega)$ are the normal Green's function bubble and the off-diagonal components $\chi_a^i(\omega)$ are the anomalous Green's function bubble. They are given by

$$\chi_n^i(\omega) = \frac{1}{4}\int \frac{d^2\boldsymbol{k}}{(2\pi)^2} \frac{|\Delta_i|^2 + 2\xi_i^2 + \xi_i \omega}{\sqrt{|\Delta_i|^2 + \xi_i^2}(|\Delta_i|^2 + \xi_i^2 - \omega^2/4)},$$
$$\chi_a^i(\omega) = -\frac{1}{4}\int \frac{d^2\boldsymbol{k}}{(2\pi)^2} \frac{|\Delta_i|^2}{\sqrt{|\Delta_i|^2 + \xi_i^2}(|\Delta_i|^2 + \xi_i^2 - \omega^2/4)}. \quad (22)$$

In the nematic SC state, the gaps on the three pockets are parametrized in terms of the four gap functions Δ_1, Δ_2, Δ_X, and Δ_Y, as discussed in Eqs. (18). Thus, we need to introduce four pairing fluctuation fields, resulting in an 8×8 bare SC

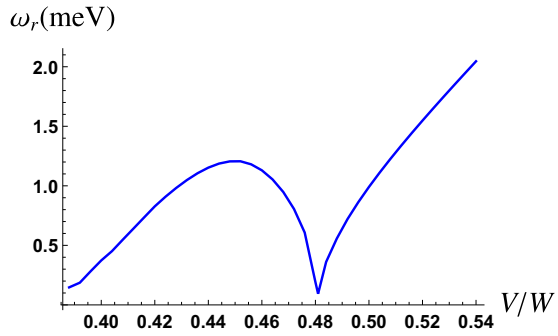

FIG. 6. Energy ω_r of the collective mode associated with the relative phase between the gaps at the X and Y pockets at $T = 0$ as function of the ratio V/W. Note that ω_r becomes soft when the transition to the time-reversal symmetry-breaking state takes place.

susceptibility matrix of the form

$$\hat{\chi}(\omega) = \begin{pmatrix} \hat{\chi}_n^h(\omega) & 0 & \hat{\chi}_a^h(\omega) & 0 \\ 0 & \hat{\chi}_n^e(\omega) & 0 & \hat{\chi}_a^e(\omega) \\ \left(\hat{\chi}_a^h\right)^\dagger(-\omega) & 0 & \hat{\chi}_n^h(-\omega) & 0 \\ 0 & \left(\hat{\chi}_a^e\right)^\dagger(-\omega) & 0 & \hat{\chi}_n^e(-\omega) \end{pmatrix}.$$

Here, the 2×2 matrices are given by

$$\hat{\chi}_\alpha^h(\omega) = \begin{pmatrix} \langle \chi_\alpha^h(\omega)\cos^4\varphi_h\rangle & \langle \chi_\alpha^h(\omega)\sin^2 2\varphi_h\rangle \\ \langle \chi_\alpha^h(\omega)\sin^2 2\varphi_h\rangle & \langle \chi_\alpha^h(\omega)\sin^4\varphi_h\rangle \end{pmatrix},$$

$$[4pt]\hat{\chi}_\alpha^e(\omega) = \begin{pmatrix} \chi_\alpha^{ex}(\omega) & 0 \\ 0 & \chi_\alpha^{ey}(\omega) \end{pmatrix}, \quad (23)$$

with $\alpha = a, n$ for anomalous and normal Green functions. $\langle\cdots\rangle$ is the average over the polar angle ϕ_h. Within RPA, the renormalized SC pairing susceptibility is then given by

$$(\hat{\chi}_R)^{-1} = (\hat{\chi})^{-1} + \hat{U}, \quad (24)$$

with

$$\hat{U} = \begin{pmatrix} 0 & \hat{U}_2 & 0 & 0 \\ \hat{U}_2 & \hat{U}_1 & 0 & 0 \\ 0 & 0 & 0 & \hat{U}_2 \\ 0 & 0 & \hat{U}_2 & \hat{U}_1 \end{pmatrix}, \quad (25)$$

and 2×2 matrices:

$$\hat{U}_1 = \begin{pmatrix} 0 & W \\ W & 0 \end{pmatrix},$$

$$\hat{U}_2 = \begin{pmatrix} V & W \\ W & V \end{pmatrix}. \quad (26)$$

Since the relative phase between Δ_X and Δ_Y assumes a nontrivial value in the TRSB state, we expect that one of the eigenmodes of $\hat{\chi}_R(\omega)$ vanishes at the transition. Of course, because we did not consider the coupling to the density, the mode of $\hat{\chi}_R(\omega)$ corresponding to the global phase is always zero, which we ignore in our analysis, as this mode becomes massive due to the Higgs mechanism. In Fig. 6, we plot the energy of the "Leggett-like" mode across the TRSB transition at $T = 0$. This mode describes fluctuations of the relative phase of the two order parameters and must soften at the critical point of an Ising second-order transition, below which this relative phase acquires an expectation value different from 0 or π. Comparing to Fig. 5, it is clear that softening occurs precisely at the boundaries delineating the regime where the nematic SC state breaks time reversal. Therefore, it follows that such a soft mode should also appear at T^*. We propose Raman experiments to verify whether such a soft mode exists in FeSe.

VI. CONCLUSIONS

In summary, we showed that the properties of FeSe favor a second SC transition at $T^* < T_c$ from a nematic $s + d$ SC state to a nematic TRS breaking $s + e^{i\alpha}d$ SC state (with $\alpha \neq 0, \pi, \pi/2$). In particular, these properties are the near degeneracy between the s-wave state and the d-wave state, the absence of competing long-range magnetic order, and a nematic state in which the nematic order paramater changes sign between electron and hole pockets. We showed that this phase transition is manifested not only in standard thermodynamic quantities, but also by softening the Legget-like mode, which can be detected by Raman spectroscopy. Furthermore, measurements such as μSR and Kerr rotation should also directly observe TRSB at T^*. It is tantalizing to attribute the recently observed peak in the specific heat at 1 K to this TRSB phase [45], although additional experiments are necessary to elucidate the origin of this peak. Finally, we note that the $s + d$ state that sets in below T_c but above T^* has been reported to be strongly anisotropic [15–20]. TRS is expected to partially suppress this anisotropy, which could also be observed experimentally.

ACKNOWLEDGMENTS

We thank B. Andersen, L. Benfatto, S. Borisenko, D. Chowdhury, L. Classen, F. Hardy, P. Hirschfeld, A. Kreisel, M. Eschrig, L. Rhodes, and M. Watson for fruitful discussions. J.K. was supported by the National High Magnetic Field Laboratory through NSF Grant No. DMR-1157490 and the State of Florida. R.M.F. and A.V.C. were supported by the U.S. Department of Energy, Office of Science, Basic Energy Sciences, under Awards No. DE-SC0012336 (R.M.F.) and No. DE-SC0014402 (A.V.C.).

APPENDIX A: BAND DISPERSION PARAMETERS

The band dispersion parameters used in our paper are given in Table I.

APPENDIX B: FREE-ENERGY EXPANSION

In this Appendix, we derive the Ginzburg-Landau coefficients coupling the nematic and SC order parameters:

$$F(\Delta) = a_s|\Delta_s|^2 + a_d|\Delta_d|^2 - (\beta_h\Phi_h + \beta_e\Phi_e)(\Delta_s^*\Delta_d + \Delta_s\Delta_d^*) + O(|\Delta|^4). \quad (B1)$$

TABLE I. Band parameters.

μ_h	N_1	N_2	Λ
13.6 meV	0.11 eV^{-1}	0.38 eV^{-1}	1.0 eV
μ_e	N_e	Φ_h	Φ_e
30 meV	0.33 eV^{-1}	10 meV	−18 meV

Although, as discussed in the main text, the nematic order parameter is not necessarily small in FeSe, this expansion allows us to gain a qualitative understanding of the differences between the cases of sign-changing and sign-preserving nematic states. The linearized BCS gap equations are given by (for simplicity, we set $\mu_h \sim \mu_e = \mu$)

$$\begin{aligned}
-\Delta_h &= N_e \ln\frac{\sqrt{\Lambda\mu_e}}{T}(V\cos^2\theta + W\sin^2\theta)\Delta_X + N_e \ln\frac{\sqrt{\Lambda\mu_e}}{T}(W\cos^2\theta + V\sin^2\theta)\Delta_Y,\\
-\Delta_X &= N_e W \ln\frac{\sqrt{\Lambda\mu_e}}{T}\Delta_Y + N_h \ln\frac{\sqrt{\Lambda\mu_h}}{T}\langle(V\cos^2\theta_h + W\sin^2\theta_h)\Delta_h\rangle_\theta,\\
-\Delta_Y &= N_e W \ln\frac{\sqrt{\Lambda\mu_e}}{T}\Delta_X + N_h \ln\frac{\sqrt{\Lambda\mu_h}}{T}\langle(V\sin^2\theta_h + W\cos^2\theta_h)\Delta_h\rangle_\theta. \qquad \text{(B2)}
\end{aligned}$$

The s-wave solution corresponds to $\Delta_X = \Delta_Y = \Delta_e^{(s)}$ and $\Delta_h = \Delta_h^{(s)}$, whereas the d-wave solution gives $\Delta_X = -\Delta_Y = \Delta_e^{(d)}$ and $\Delta_h = \Delta_h^{(d)}\cos 2\theta_h$. In terms of these parametrizations, the coupled gap equations become

$$\begin{pmatrix} \lambda_s(V+W) & 1 \\ 1+\lambda_s W & \frac{N_h}{N_e}\lambda_s\frac{V+W}{2}\end{pmatrix}\begin{pmatrix}\Delta_e^{(s)}\\ \Delta_h^{(s)}\end{pmatrix} = 0, \qquad \text{(B3)}$$

and

$$\begin{pmatrix} \lambda_d(V-W) & 1 \\ 1-\lambda_d W & \frac{N_h}{N_e}\lambda_d\frac{V-W}{4}\end{pmatrix}\begin{pmatrix}\Delta_e^{(d)}\\ \Delta_h^{(d)}\end{pmatrix} = 0, \qquad \text{(B4)}$$

where we defined the coupling constants $\lambda_{(s,d)} = N_e \ln\frac{\sqrt{\Lambda\mu}}{T_{(s,d)}}$. The ratios between Δ_h and Δ_e in the s- and d-wave channels, defined as $\alpha_{(s,d)} = \Delta_h^{(s,d)}/\Delta_e^{(s,d)}$, can be readily extracted from the equations above. We have $\alpha_s = -\lambda_s(V+W) < 0$, corresponding to an s^{+-} state, and $\alpha_d = \lambda_d(W-V) > 0$, corresponding to a d^{++} state (recall that the d-wave state takes place only when $V < W$).

To compute the coupling constants β_e and β_h in Eq. (B1), we first calculate the coefficients γ_e and γ_h defined by

$$\begin{aligned}
\delta F_e &= -\gamma_e\Phi_e(|\Delta_X|^2 - |\Delta_Y^2|),\\
\delta F_h &= -\gamma_h\Phi_h\left(\Delta_h^{(s)^*}\Delta_h^{(d)} + \text{c.c}\right). \qquad \text{(B5)}
\end{aligned}$$

Straightforward calculation of the triangular Feynman diagrams gives

$$\begin{aligned}
\gamma_e &= 2N_e\frac{1-2n_f(\mu)}{2\mu} > 0,\\
\gamma_h &= -N_h\frac{1-2n_f(\mu_h)}{2\mu_h} < 0. \qquad \text{(B6)}
\end{aligned}$$

Now, using the fact that $|\Delta_X|^2 - |\Delta_Y|^2 = (\Delta_e^{(s)^*}\Delta_e^{(d)} + \text{c.c})$, and the results $\Delta_h^{(s,d)} = \alpha_{(s,d)}\Delta_e^{(s,d)}$ derived above, we arrive at

$$\delta F = -(\gamma_h\alpha_s\alpha_d\Phi_h + \gamma_e\Phi_e)\left(\Delta_e^{(s)^*}\Delta_e^{(d)} + \text{c.c}\right) \qquad \text{(B7)}$$

Therefore, we can identify $\beta_h = \gamma_h\alpha_s\alpha_d$ and $\beta_e = \gamma_e$. Since $\gamma_e, \alpha_d > 0$ and $\gamma_h, \alpha_s < 0$, it follows that $\beta_h, \beta_e > 0$. We checked that inclusion of the contributions arising from the changes in the pairing interaction caused by nematicity does not alter this result.

[1] See, e.g., A. Böhmer and A. Kreisel, J. Phys.: Condens. Matter **30**, 023001 (2017), and references therein.

[2] S.-H. Baek, D. V. Efremov, J. M. Ok, J. S. Kim, J. van den Brink, and B. Buchner, Nat. Mater. **14**, 210 (2015).

[3] A. E. Bohmer, T. Arai, F. Hardy, T. Hattori, T. Iye, T. Wolf, H. V. Lohneysen, K. Ishida, and C. Meingast, Phys. Rev. Lett. **114**, 027001 (2015).

[4] A. V. Chubukov, M. Khodas, and R. M. Fernandes, Phys. Rev. X **6**, 041045 (2016).

[5] A. V. Chubukov, R. M. Fernandes, and J. Schmalian, Phys. Rev. B **91**, 201105 (2015).

[6] R. Yu and Q. Si, Phys. Rev. Lett. **115**, 116401 (2015).

[7] Z. Wang, W.-J. Hu, and A. H. Nevidomskyy, Phys. Rev. Lett. **116**, 247203 (2016).

[8] F. Wang, S. A. Kivelson, and D.-H. Lee, Nat. Phys. **11**, 959 (2015).

[9] K. Jiang, J. Hu, H. Ding, and Z. Wang, Phys. Rev. B **93**, 115138 (2016).

[10] J. K. Glasbrenner, I. I. Mazin, H. O. Jeschke, P. J. Hirschfeld, R. M. Fernandes, and R. Valenti, Nat. Phys. **11**, 953 (2015).

[11] K. Matsuura, Y. Mizukami, Y. Arai, Y. Sugimura, N. Maejima, A. Machida, T. Watanuki, T. Fukuda, T. Yajima, Z. Hiroi, K. Y. Yip, Y. C. Chan, Q. Niu, S. Hosoi, K. Ishida, K. Mukasa, T. Watashige, S. Kasahara, J.-G. Cheng, S. K. Goh, Y. Matsuda, Y. Uwatoko, and T. Shibauchi, Nat. Commun. **8**, 1143 (2017).

[12] L. Xiang, U. S. Kaluarachchi, A. E. Böhmer, V. Taufour, M. A. Tanatar, R. Prozorov, S. L. Bud'ko, and P. C. Canfield, Phys. Rev. B **96**, 024511 (2017).

[13] F.-C. Hsu, J.-Y. Luo, K.-W. Yeh, T.-K. Chen, T.-W. Huang, Ph. M. Wu, YongChi Lee, Y.-L. Huang, Y.-Y. Chu, Der-Chung Yan, and Maw-Kuen Wu, Proc. Natl. Acad. Sci. USA **105**, 14262 (2008).

[14] T. M. McQueen, A. J. Williams, P. W. Stephens, J. Tao, Y. Zhu, V. Ksenofontov, F. Casper, C. Felser, and R. J. Cava, Phys. Rev. Lett. **103**, 057002 (2009).

[15] H. C. Xu, X. H. Niu, D. F. Xu, J. Jiang, Q. Yao, Q. Y. Chen, Q. Song, M. Abdel-Hafiez, D. A. Chareev, A. N. Vasiliev, Q. S. Wang, H. L. Wo, J. Zhao, R. Peng, and D. L. Feng, Phys. Rev. Lett. **117**, 157003 (2016).

[16] T. Hashimoto, Y. Ota, H. Q. Yamamoto, Y. Suzuki, T. Shimojima, S. Watanabe, C. Chen, S. Kasahara, Y. Matsuda, T. Shibauchi, K. Okazaki, and S. Shin, Nat. Commun. **9**, 282 (2018).

[17] Y. S. Kushnirenko, A. V. Fedorov, E. Haubold, S. Thirupathaiah, T. Wolf, S. Aswartham, I. Morozov, T. K. Kim, B. Büchner, and S. V. Borisenko, Phys. Rev. B **97**, 180501 (2018)

[18] D. Liu, C. Li, J. Huang, B. Lei, L. Wang, X. Wu, B. Shen, Q. Gao, Y. Zhang, X. Liu, Y. Hu, Y. Xu, A. Liang, J. Liu, P. Ai, L. Zhao, S. He, Li Yu, G. Liu, Y. Mao, X. Dong, X. Jia, F. Zhang, S. Zhang, F. Yang, Z. Wang, Q. Peng, Y. Shi, J. Hu, T. Xiang, X. Chen, Z. Xu, C. Chen, and X. J. Zhou, Phys. Rev. X **8**, 031033 (2018).

[19] L. C. Rhodes, M. D. Watson, A. A. Haghighirad, D. V. Evtushinsky, M. Eschrig, and T. K. Kim, arXiv:1804.01436.

[20] P. O. Sprau, A. Kostin, A. Kreisel, A. E. Böhmer, V. Taufour, P. C. Canfield, S. Mukherjee, P. J. Hirschfeld, B. M. Andersen, and J. C. Séamus Davis, Science **357**, 75 (2017); see also A. Kostin, P. O. Sprau, A. Kreisel, Y.-X. Chong, A. E. Böhmer, P. C. Canfield, P. J. Hirschfeld, B. M. Andersen, and J. C. Séamus Davis, arXiv:1802.02266.

[21] L. Jiao, C.-L. Huang, S. Rößler, C. Koz, U. K. Rößler, U. Schwarz, and S. Wirth, Sci. Rep. **7**, 44024 (2017).

[22] T. Hanaguri, K. Iwaya, Y. Kohsaka, T. Machida, T. Watashige, S. Kasahara, T. Shibauchi, and Y. Matsuda, Sci. Adv. **4**, eaar6419 (2018).

[23] P. Bourgeoi-Hope, S. Chi, D. A. Bonn, R. Liang, W. N. Hardy, T. Wolf, C. Meingast, N. Doiron-Leyraud, and L. Taillefer, Phys. Rev. Lett. **117**, 097003 (2016).

[24] L. Wang, F. Hardy, T. Wolf, P. Adelmann, R. Fromknecht, P. Schweiss, and C. Meingast, Phys. Status Solidi B **254**, 1600153 (2017).

[25] Y. Sato, S. Kasahara, T. Taniguchi, X. Z. Xing, Y. Kasahara, Y. Tokiwa, T. Shibauchi, and Y. Matsuda, Proc. Natl. Acad. Sci. USA **115**, 1227 (2018).

[26] S. Mukherjee, A. Kreisel, P. J. Hirschfeld, and B. M. Andersen, Phys. Rev. Lett. **115**, 026402 (2015).

[27] A. Kreisel, B. M. Andersen, P. O. Sprau, A. Kostin, J. C. Séamus Davis, P. J. Hirschfeld, Phys. Rev. B **95**, 174504 (2017).

[28] J. Kang, R. M. Fernandes, and A. V. Chubukov, Phys. Rev. Lett. **120**, 267001 (2018).

[29] L. Benfatto, B. Valenzuela, and L. Fanfarillo, arXiv:1804.05800.

[30] S. Maiti, M. M. Korshunov, T. A. Maier, P. J. Hirschfeld, and A. V. Chubukov, Phys. Rev. B **84**, 224505 (2011); Phys. Rev. Lett. **107**, 147002 (2011); S. Maiti, M. M. Korshunov, and A. V. Chubukov, Phys. Rev. B **85**, 014511 (2012).

[31] W.-C. Lee, S.-C. Zhang, and C. Wu, Phys. Rev. Lett. **102**, 217002 (2009).

[32] V. Stanev and Z. Tesanovic, Phys. Rev. B **81**, 134522 (2010).

[33] C. Platt, R. Thomale, C. Honerkamp, S.-C. Zhang, and W. Hanke, Phys. Rev. B **85**, 180502(R) (2012).

[34] R. M. Fernandes and A. J. Millis, Phys. Rev. Lett. **111**, 127001 (2013).

[35] M. Khodas and A. V. Chubukov, Phys. Rev. Lett. **108**, 247003 (2012).

[36] J. Kang, A. F. Kemper, and R. M. Fernandes, Phys. Rev. Lett. **113**, 217001 (2014).

[37] G. Livanas, A. Aperis, P. Kotetes, and G. Varelogiannis, Phys. Rev. B **91**, 104502 (2015).

[38] R. M. Fernandes and A. J. Millis, Phys. Rev. Lett. **110**, 117004 (2013).

[39] D. W. Tam, T. Berlijn, and T. A. Maier, Phys. Rev. B **98**, 024507 (2018)

[40] J.-H. She, M. J. Lawler, and E.-A. Kim, arXiv:1701.07813.

[41] Z.-X. Li, F. Wang, H. Yao, and D.-H. Lee, Sci. Bull. **61**, 925 (2016).

[42] Q. Wang, Y. Shen, B. Pan, Y. Hao, M. Ma, F. Zhou, P. Steffens, K. Schmalzl, T. R. Forrest, M. Abdel-Hafiez, X. Chen, D. A. Chareev, A. N. Vasiliev, P. Bourges, Y. Sidis, and H. Cao, Nat. Mater. **15**, 159 (2016).

[43] Y. Yamakawa, S. Onari, and H. Kontani, Phys. Rev. X **6**, 021032 (2016).

[44] Y. Suzuki, T. Shimojima, T. Sonobe, A. Nakamura, M. Sakano, H. Tsuji, J. Omachi, K. Yoshioka, M. Kuwata-Gonokami, T. Watashige, R. Kobayashi, S. Kasahara, T. Shibauchi, Y. Matsuda, Y. Yamakawa, H. Kontani, and K. Ishizaka, Phys. Rev. B **92**, 205117 (2015).

[45] G.-Y. Chen, X. Zhu, Huan Yang, and Hai-Hu Wen, Phys. Rev. B **96**, 064524 (2017).

[46] M. D. Watson, T. K. Kim, A. A. Haghighirad, N. R. Davies, A. McCollam, A. Narayanan, S. F. Blake, Y. L. Chen, S. Ghannadzadeh, A. J. Schofield, M. Hoesch, C. Meingast, T. Wolf, and A. I. Coldea, Phys. Rev. B **91**, 155106 (2015).

[47] A. I. Coldea and M. D. Watson, Annu. Rev. Condens. Matter Phys. **9**, 125 (2018).

[48] A. Fedorov, A. Yaresko, T. K. Kim, E. Kushnirenko, E. Haubold, T. Wolf, M. Hoesch, A. Grueneis, B. Buechner, and S. V. Borisenko, Sci. Rep. **6**, 36834 (2016).

[49] R. M. Fernandes and A. V. Chubukov, Rep. Prog. Phys. **80**, 014503 (2017).

[50] V. Cvetkovic and O. Vafek, Phys. Rev. B **88**, 134510 (2013).

[51] L. Classen, R.-Q. Xing, M. Khodas, and A. V. Chubukov, Phys. Rev. Lett. **118**, 037001 (2017).

[52] L. Fanfarillo, G. Giovannetti, M. Capone, and E. Bascones, Phys. Rev. B **95**, 144511 (2017).

[53] L. de Medici, G. Giovannetti, and M. Capone, Phys. Rev. Lett. **112**, 177001 (2014).

[54] Z. P. Yin, K. Haule, and G. Kotliar, Nat. Mater. **10**, 932 (2011).

[55] R. M. Fernandes and O. Vafek, Phys. Rev. B **90**, 214514 (2014).

[56] O. Vafek and A. V. Chubukov, Phys. Rev. Lett. **118**, 087003 (2017).

[57] L. Fanfarillo, J. Mansart, P. Toulemonde, H. Cercellier, P. Le Fevre, F. Bertran, B. Valenzuela, L. Benfatto, and V. Brouet, Phys. Rev. B **94**, 155138 (2016).

[58] T. Watashige, Y. Tsutsumi, T. Hanaguri, Y. Kohsaka, S. Kasahara, A. Furusaki, M. Sigrist, C. Meingast, T. Wolf, H. V. Lohneysen, T. Shibauchi, and Y. Matsuda, Phys. Rev. X **5**, 031022 (2015).